Research Article | Vol. 27, No. 6 | 18 Mar 2019 | OPTICS EXPRESS 8745
Optics EXPRESS

Fs-laser-written thulium waveguide lasers Q-switched by graphene and MoS_2

ESROM KIFLE,[1] PAVEL LOIKO,[2] JAVIER RODRÍGUEZ VÁZQUEZ DE ALDANA,[3] CAROLINA ROMERO,[3] AIRAN RÓDENAS,[1,4] VIKTOR ZAKHAROV,[2] ANDREY VENIAMINOV,[2] HAOHAI YU,[5] HUAIJIN ZHANG,[5] YANXUE CHEN,[6] MAGDALENA AGUILÓ,[1] FRANCESC DÍAZ,[1] UWE GRIEBNER,[7] VALENTIN PETROV,[7] AND XAVIER MATEOS[1,*]

[1]*Universitat Rovira i Virgili, Departament Química Física i Inorgànica, Física i Cristal·lografia de Materials i Nanomaterials (FiCMA-FiCNA)-EMaS, Campus Sescelades, E-43007 Tarragona, Spain*
[2]*ITMO University, 49 Kronverkskiy Pr., 197101 St. Petersburg, Russia*
[3]*Aplicaciones del Láser y Fotónica, University of Salamanca, 37008 Salamanca, Spain*
[4]*Istituto di Fotonica e Nanotecnologie, Consiglio Nazionale delle Ricerche (IFN-CNR), Piazza Leonardo da Vinci, 32, 20133 Milano, Italy*
[5]*State Key Laboratory of Crystal Materials and Institute of Crystal Materials, Shandong University, 250100 Jinan, China*
[6]*School of Physics, Shandong University, 250100 Jinan, China*
[7]*Max Born Institute for Nonlinear Optics and Short Pulse Spectroscopy, Max-Born-Str. 2a, D-12489 Berlin, Germany*
**xavier.mateos@urv.cat*

Abstract: We report the generation of mid-infrared (~2 μm) high repetition rate (MHz) sub-100 ns pulses in buried thulium-doped monoclinic double tungstate crystalline waveguide lasers using two-dimensional saturable absorber materials, graphene and MoS_2. The waveguide (propagation losses of ~1 dB/cm) was micro-fabricated by means of ultrafast femtosecond laser writing. In the continuous-wave regime, the waveguide laser generated 247 mW at 1849.6 nm with a slope efficiency of 48.7%. The laser operated at the fundamental transverse mode with a linearly polarized output. With graphene as a saturable absorber, the pulse characteristics were 88 ns / 18 nJ (duration / energy) at a repetition rate of 1.39 MHz. Even shorter pulses of 66 ns were achieved with MoS_2. Graphene and MoS_2 are therefore promising for high repetition rate nanosecond Q-switched infrared waveguide lasers.

1. Introduction

Waveguide (WG) lasers emitting in the spectral range of ~2 μm are of interest for spectroscopy, telecom and environmental sensing applications [1]. This is because their emission is eye-safe and matches the absorption lines of various atmospheric and bio-molecules. The laser operation at ~2 μm is achieved using such trivalent rare-earth ions as Thulium (Tm^{3+}) or Holmium (Ho^{3+}). In the former case, the transition of interest is $^3F_4 \rightarrow {}^3H_6$. Due to the large Stark splitting of the Tm^{3+} ground-state, its emission is wavelength-tunable. The Tm^{3+} ions feature strong absorption at ~0.8 μm ($^3H_6 \rightarrow {}^3H_4$ transition) allowing for their efficient pumping by AlGaAs laser diodes and Ti:Sapphire lasers. Moreover, the cross-relaxation for adjacent Tm^{3+} ions, $^3H_4 + {}^3H_6 \rightarrow {}^3F_4 + {}^3F_4$, can potentially raise the pump quantum efficiency up to 2.

Efficient continuous-wave (CW) thulium WG lasers are known [2,3]. Several methods have been used to fabricate WGs based on Tm^{3+}-doped materials, e.g., liquid phase epitaxy (LPE) in combination with ion beam etching [2], optical bonding [4], ion diffusion [5], reactive co-sputtering [6] and femtosecond direct laser writing (fs-DLW) also referred as ultrafast laser inscription (ULI) [7]. In the latter approach, the output of an ultrafast (fs)

#357738 https://doi.org/10.1364/OE.27.008745
Journal © 2019 Received 23 Jan 2019; accepted 18 Feb 2019; published 11 Mar 2019

Optics EXPRESS

amplifier is tightly focused in a transparent laser material causing a permanent variation of its refractive index. An inscription of a three-dimensional structure may thus lead to the waveguiding behaviour. Fs-DLW is attractive because it allows one to fabricate a variety of photonic microstructures [8,9] in different materials (from glasses to crystals and ceramics).

Less attention has been paid to pulsed (Q-switched and mode-locked) thulium WG lasers. In particular, passive Q-switching is realized by insertion into the laser cavity of a nonlinear optical element – saturable absorber (SA) – showing increasing (bleachable) transmission for high laser fluence / intensity.

For the spectral range of ~2 μm, there exist two types of SAs. The first type ("slow" SAs) includes transition-metal -doped crystals, e.g., Cr^{2+}:ZnS or Cr^{2+}:ZnSe [10]. The second one ("fast" SAs) includes semiconductor saturable absorber mirrors (SESAMs) and nanostructures based on two-dimensional (2D) few-atomic layer materials, e.g., graphene [11], single-walled carbon nanotubes (SWCNTs) [12] and transition metal dichalcogenides (TMDs) [13]. When employed in a passively Q-switched (PQS) laser, "fast" SAs provide the generation of nanosecond (ns) pulses at high repetition rates in the range of hundreds of kHz – few MHz.

Graphene is the most prominent example of 2D materials. It consists of a single layer of carbon atoms arranged in a honeycomb lattice. Graphene features hollow cone valence and conduction bands meeting each other at the Dirac point. Such a zero band gap electronic structure leads to wavelength-independent small-signal absorption of graphene ($\pi\alpha \approx 2.3\%$, $\alpha = e^2/\hbar c \approx 1/137$ is the fine structure constant) [14]. Moreover, graphene exhibits broadband (0.8 – 3 μm) saturable absorption due to the finite number of electron and hole states according to the Pauli blocking principle [11,15]. The low-signal absorption is almost independent of the photon energy $h\nu$, but the saturation intensity of graphene I_{sat} increases with $h\nu$ due to the band structure [16]. Thus, the application of graphene as a saturable absorber (SA) in lasers emitting at ~2 μm is of particular interest [17]. As a SA, graphene offers relatively low I_{sat}, ultrafast recovery time and sufficiently high laser-induced damage threshold.

The success of graphene SAs stimulated the study of other 2D materials containing few atomic layers and exhibiting broadband linear and nonlinear absorption such as, e.g., TMDs, MX_2 where M = Mo or W and X = S, Se or Te. For TMDs, one layer of M atoms is sandwiched between two layers of X atoms and the adjacent layers are bound by weak Van-der-Waals forces. Molybdenum disulfide (MoS_2) is one of the most studied TMDs [13,18]. TMDs offer a higher fraction of the saturable absorption as compared to graphene [19]. Both graphene and MoS_2 can be used in transmission-type and evanescent-field-based SAs.

Table 1. Laser Performance* of PQS Thulium Waveguide Lasers Reported So Far

Material	Fabrication	SA	P_{out}, mW	η, %	$\Delta\tau$, ns	E_{out}, nJ	PRF, kHz	Ref.
Tm:ZBLAN glass	fs-DLW	graphene	6	~5	2760	240	25	[20]
Tm:ZBLAN glass	fs-DLW	Bi_2Te_3	16.3	1.3	1400	370	44.1	[21]
Tm:YAG	fs-DLW	graphene	6.5	~2	<500	9.5	684	[22]
Tm:$KLu(WO_4)_2$	fs-DLW	SWCNTs	10.3	3.8	50	7	1480	[23]
Tm:$KY(WO_4)_2$	LPE	Cr^{2+}:ZnS	1.2	~3	1200	120	10	[24]
Tm:$KY(WO_4)_2$	LPE	SWCNTs	45.6	22.5	83	33	1390	[25]

*P_{out} – average output power, η – slope efficiency, $\Delta\tau$ – pulse duration, E_{out} – pulse energy, PRF – pulse repetition frequency.

An overview of PQS thulium WG lasers reported to date is presented in Table 1. Regarding planar WG lasers produced by LPE, a "slow" SA (Cr^{2+}:ZnS) was employed in a Tm:$KY(WO_4)_2$ laser yielding 1.2 μs / 0.12 μJ (duration / energy) pulses at a low repetition rate of 10 kHz [24]. The use of a "fast" SWCNT-based SA in a similar laser lead to much shorter pulses of 83 ns / 33 nJ at 1.39 MHz [25]. However, both these lasers generated spatially multimode output.

Optics EXPRESS

As for channel WGs produced by fs-DLW, solely "fast" SAs have been used, incl. graphene, topological insulator (Bi_2Te_3) and SWCNTs [20–23]. Typically, these lasers generated µs-long pulses with a low average output power. In [20], a fs-DLW Tm:ZBLAN glass WG laser was passively Q-switched by a graphene-SA yielding 2.76 µs / 0.24 µJ pulses at a repetition rate of 25 kHz. The output power of this laser was 6 mW at ~1.9 µm with a slope efficiency of only 5%. MoS_2 has never been used in Tm WG lasers yet, to the best of our knowledge.

In the present work, we employ few-atomic-layer graphene and MoS_2 as saturable absorbers in fs-DLW Thulium channel WG lasers based on a monoclinic crystal, for the first time, to the best of our knowledge. We demonstrate the generation of sub-100 ns pulses from such lasers at MHz repetition rates.

2. Experimental

2.1. Femtosecond-laser-written waveguide

A depressed-index channel WG with a circular cladding was fabricated by fs-DLW in a bulk monoclinic crystal of Tm:KLu$(WO_4)_2$ (shortly KLuW) [23]. The crystal itself was grown by the Top-Seeded Solution Growth (TSSG) Slow-Cooling method using potassium ditungstate ($K_2W_2O_7$) as a flux and a [010]-oriented seed [26]. It was doped with 3 at.% Tm^{3+} (N_{Tm} = 2.15 × 10^{20} at/cm^3). The crystal was oriented along the N_g axis of the optical indicatrix (length: 3.0 mm, aperture: 3.10(N_m) × 2.85(N_p) mm^2). For the inscription, a Ti:Sapphire regenerative amplifier emitting 120 fs pulses at 795 nm at a repetition rate of 1 kHz was used. The laser beam was focused into the crystal using a 40 × microscope objective (N.A. = 0.65). The incident pulse energy was 57 nJ. The crystal was scanned at 400 µm/s along its N_g-axis producing damage tracks. The WG consisted of a 40 µm diameter core and a ring of damage tracks forming a cladding. The axis of the WG was located at 120 µm below the crystal surface. The separation between adjacent tracks was 2 µm. The estimated variation of the refractive index in the cladding was ~6 × 10^{-4} [27].

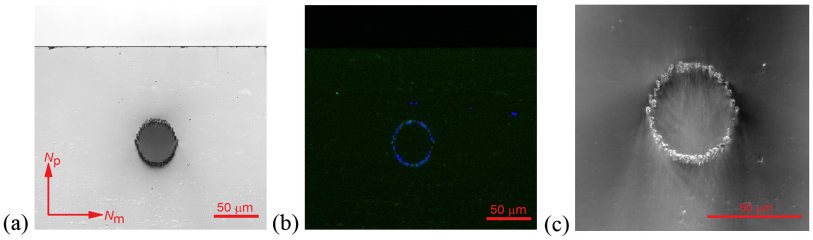

Fig. 1. Confocal laser microscope images of the laser-grade-polished end-face of the Tm:KLuW WG: (a) transmission mode, polarized light (P || N_p), λ = 405 nm; (b) back-propagating luminescence, unpolarized light, natural color, λ_{exc} = 405 nm; (c) transmission mode, crossed polarizers (P || N_p, A || N_m), λ = 488 nm.

To characterize the WG, we employed confocal laser microscopy (LSM 710, Carl Zeiss). First, one of the polished WG end-faces was studied. In transmission mode with polarized light, a dark ring of damage tracks below the crystal surface representing the cladding was observed, Fig. 1(a). No cracks surrounding the cladding are visible for the selected pulse energy. The cladding exhibits a blue emission related to color centers, Fig. 1(b), confirming the modification of the material in this region.

With the help of crossed polarizers, the birefringence of the laser-written tracks forming the cladding was revealed. Fs-DLW induces a spatially localized modification of the material compromising its crystallinity and therefore its index of refraction, as well as inducing anisotropic stress fields surrounding each laser-written track [28]. The latter will result in a local variation of the optical indicatrix due to the photo-elastic effect leading to an additional phase shift for rays propagating through such a structure. KLuW is optically biaxial so that

Optics EXPRESS

with a crossed polarizer (P) and an analyzer (A) oriented along the optical indicatrix axes, Fig. 1(c), no transmitted light is expected. One can see a bright ring of damage tracks and weaker distributed "flows" in the core and in the surrounding area induced by the stress fields. They are symmetric with respect to the vertical direction (direction of propagation of the writing laser).

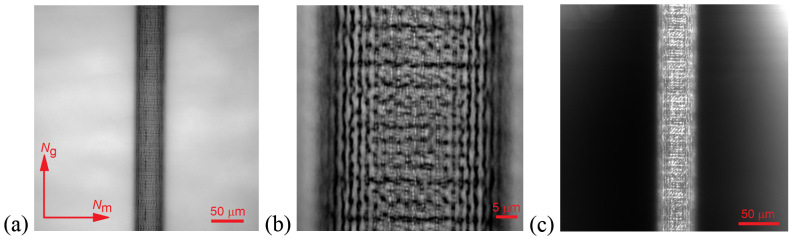

Fig. 2. Confocal laser microscope images (top view) of the central part of the circular cladding WG in Tm:KLuW: (a,b) transmission mode, polarized light (P || N_g), λ = 405 nm; (c) transmission mode, crossed polarizers (P || N_g, A || N_m), λ = 488 nm.

Similarly, observing the WG from the top crystal surface, in Fig. 2(a), a dark barrel-shaped cladding is visible in the unmodified bulk material. The cladding has a periodic net-like surface, Fig. 2(b), that may be related to defects in the motion of the micro-positioning stage during fabrication. Both these measurements were done in transmission mode with polarized light. With crossed polarizers, a bright cladding is visible in a dark crystal, Fig. 2(c), indicating a notable birefringence.

2.2. Laser set-up

The laser experiments were performed under pumping by a Ti:Sapphire laser (Coherent, model Mira 900) tuned to 802 nm ($^3H_6 \rightarrow {}^3H_4$ Tm^{3+} transition). The pump beam was linearly polarized (polarization in the crystal: $\boldsymbol{E}$ || N_m). The pump radiation was coupled into the WG using a microscope objective (Mitutoyo M Plan NIR 10 × , numerical aperture, N.A.: 0.28, focal length, f = 20 mm, working distance: 30.5 mm). The pump spot size $2w_P$ on the input facet of the WG was 40 ± 5 μm. The measured pump coupling efficiency η_{coupl} was 81 ± 2% (as determined from pump-transmission measurements performed at ~0.83 μm, out of Tm^{3+} absorption) including the Fresnel losses at the uncoated WG facet and the measured pump absorption under lasing conditions $\eta_{abs,L}$ was 75 ± 2%. The incident pump power was varied with a gradient neutral density (ND) filter (Thorlabs, NDC-50C-4M) placed before the objective.

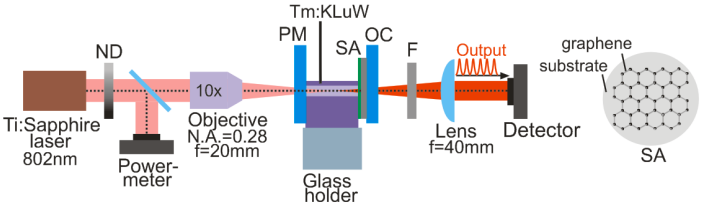

Fig. 3. Laser set-up: ND – gradient neutral-density filter, PM – pump mirror, SA – saturable absorber, OC – output coupler, F – cut-off filter.

External (bulk) cavity mirrors were used. The laser cavity consisted of a flat pump mirror (PM) that was anti-reflection (AR) coated for 0.7–1.0 μm and highly-reflective (HR) coated for 1.8–2.1 μm and a flat output coupler (OC) having a transmission T_{OC} of 20% or 30% at 1.8–2.1 μm. The crystal was passively-cooled and mounted on a BK7 glass substrate. Its input face was placed close to the PM. Between the crystal and the OC, a transmission-type SA was inserted for PQS operation (at normal incidence). All optical elements were separated by

minimum air gaps. No index-matching liquid was used to avoid damage of optical elements. The geometrical cavity length was 4.0 mm.

The laser output was filtered from the residual pump with a long-pass filter (FEL1000, Thorlabs). The spectrum of the laser emission was measured using an optical spectrum analyser (OSA, Yokogawa, AQ6375B) and the near-field beam profile was captured using a plano-convex lens (f = 40 mm) and a FIND-R-SCOPE near-IR camera. The crystal was replaced by a 1951 USAF resolution test target (R1DS1, Thorlabs) to determine the mode size at the OC.

2.3. Saturable absorbers

Two transmission-type SAs were studied. Both of them were deposited on a laser-grade-polished quartz substrate (thickness: 1.0 mm). The first SA was based on a commercial large-area multi-layer chemical vapor deposition (CVD) graphene. Its small-signal transmission T_{SA} measured at the laser wavelength of ~1.85 μm was 94.3% (the initial (non-saturated) absorption $\alpha'_{SA} = 1 - T_{SA}$ was 5.7%). For a single-layer graphene deposited at the same conditions, $\alpha'_{SA} \approx 2.3\%$, in good agreement with the theoretical value. Thus, the sample contained between 2 and 3 carbon layers (n) deposited layer-by-layer. The saturable absorption $\alpha'_S = 0.24\%$ (at ~1.85 μm) and the saturation intensity $I_{sat} = 0.6$ MW/cm^2 (at ~2 μm). We describe the saturation of the graphene-SA by the "fast" SA model [19]:

$$\alpha'(I) = \alpha'_{NS} + \frac{\alpha'_S}{1 + (I / I_{sat})}, \quad \alpha'_{SA} = 1 - T_{SA} = \alpha'_{NS} + \alpha'_S. \tag{1}$$

Here, $\alpha'(I)$ is the actual absorption and I is the light intensity. Multi-carbon-layer graphene-SA was selected in order to increase the saturable absorption (α'_S) which is raising with the number of graphene layers [16]. As a competing detrimental process, with the increase of n, the fraction of the saturable loss to the small-signal absorption (α'_S/α'_{SA}) is decreasing due to enhanced scattering at the layer-to-layer interfaces. In [29], a graphene-SA containing three carbon layers shown the best PQS performance at ~2 μm.

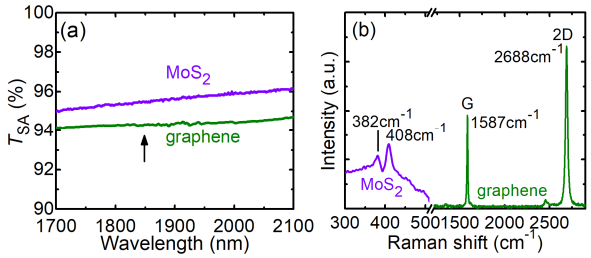

Fig. 4. Graphene- and MoS_2-SAs: (a) small-signal transmission spectra, (b) Raman spectra, λ_{exc} = 514 nm. The *arrow* in (a) corresponds to the laser wavelength.

The second SA was based on a MoS_2 film prepared by pulsed laser deposition (PLD) using polycrystalline MoS_2 [19]. Its characteristics were as follows: $T_{SA} = 95.5\%$, $\alpha'_S = 0.33\%$ and I_{sat} ~0.5 MW/cm^2. The measured MoS_2 film thickness was 20 nm, thus containing about 30 MoS_2 layers if considering an individual layer thickness of ~0.65 nm and their bonding by Van der Waals interaction.

The small-signal internal transmission (T(SA + substrate)/T(substrate)) spectra as well as the Raman spectra of both SAs are shown in Fig. 4.

Raman spectroscopy is a sensitive method to characterize few-atomic layer materials. In the Raman spectrum of graphene-SA, two intense bands centered at 1587 cm^{-1} (G) and 2688 cm^{-1} (2D) are observed. The increase of the number of carbon layers affects the Raman spectra, i.e., it modifies the spectral shape of the 2D band and the intensity ratio of the 2D and G ones [30,31]. In our case, I(2D)/I(G) = 1.73 which is lower than for the single-layer

Optics EXPRESS

graphene (I(2D)/I(G) = 2.2). The position of the 2D band corresponds to n between 2 and 3. In the Raman spectrum of the MoS_2-SA, two characteristic bands at 382 cm^{-1} (E^1_{2g}) and 408 cm^{-1} (A_{1g}) [32] are observed. The former one is assigned to the motion of the Mo + S atoms in the x-y layered plane of the unit cell.

3. Results and discussion

3.1. Continuous-wave laser

Without the SA in the cavity, we studied the laser performance in the continuous-wave (CW) mode, see Fig. 5. The maximum output power reached 247 mW at 1849.6 nm corresponding to a slope efficiency η of 48.7% *vs*. the absorbed pump power P_{abs} (for 30% OC). The optical-to-optical efficiency *vs*. the incident pump power η_{opt} was 38.4%. For 20% OC, the laser generated 184.3 mW at 1851.4 nm with lower η = 35.9% and η_{opt} = 28.8%. The laser thresholds were at P_{abs} = 41 mW and 45 mW for 20% and 30% OCs, respectively. The input-output dependences were clearly linear representing no detrimental thermal effects; no thermal fracture nor damage of the WG facets were observed.

The WG propagation (passive) loss δ_{loss} was estimated using the Caird analysis [33] (taking into account the laser performance at low output coupling [23]) as ~1.0 ± 0.3 dB/cm.

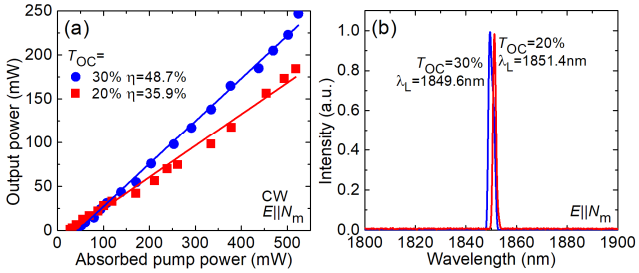

Fig. 5. CW Tm:KLuW channel WG laser: (a) input-output dependences, η – slope efficiency; (b) typical laser emission spectra (measured at P_{abs} = 0.52 W).

The laser emission was linearly polarized, $\boldsymbol{E} \parallel N_m$, the polarization was naturally-selected by the anisotropy of the gain. The typical laser emission spectra are presented in Fig. 5(b). The full width at half maximum (FWHM, 3 dB bandwidth) of the spectra is 1.4 nm and 2.4 nm for T_{OC} = 20% and 30%, respectively.

Table 2. CW Laser Performance* of Fs-Laser-Written Thulium Waveguides Reported So Far

Material	Form	Pump	λ_p, nm	P_{th}, mW	P_{out}, mW	λ_L, nm	η, %	η_{coupl}, %	δ_{loss}, dB/cm	Ref.
Tm:ZBLAN	glass	Diode	791	265	60	~1900	54^{Abs}	77	0.2 ± 0.1	[7]
Tm:ZBLAN	glass	Ti:Sa	790	**12**	205	1890	$\mathbf{67}^{Abs}$	79	0.4 ± 0.2	[34]
Tm:GPNG	glass	Ti:Sa	791	80	32	1930	6^{Inc}	4	0.7 ± 0.3	[35]
Tm:YAG	ceramics	Ti:Sa	800	312	93.2	1985	27^{Inc}	20	–	[36]
Tm:Lu_2O_3	ceramics	Ti:Sa	796	50	81	1942	7^{Inc}	40	0.7 ± 0.3	[37]
Tm:YAG^t	crystal	Ti:Sa	-	100	48	1985	12^{Inc}	9	–	[38]
Tm:KLuW	crystal	Ti:Sa	802	**41**	**247**	1850	$\mathbf{49}^{Abs}$	81	1.0 ± 0.3	**

*λ_P – pump wavelength, P_{th} – laser threshold, P_{out} – output power, λ_L – laser wavelength, η – slope efficiency (superscript: calculated vs. the incident (*Inc*) or absorbed (*Abs*) pump power), η_{coupl} – pump coupling efficiency, δ_{loss} – propagation loss. **This work.

In Table 2, we compared the CW performance of fs-DLW thulium WGs lasers reported to date (the best results were selected from multiple publications on the same material). Fs-DLW was employed for microstructuring of Tm^{3+}-doped fluoride glasses (ZBLAN, GPNG), oxide ceramics (based on cubic YAG and Lu_2O_3) and crystals (YAG). All these materials are optically isotropic. Using a WG written in monoclinic (anisotropic) Tm:KLuW crystal, we

Optics EXPRESS

have achieved the highest output power, the lowest laser threshold and the highest slope efficiency for any ceramic / crystalline material.

3.2. Passively Q-switched laser

Passive Q-switching of the Tm WG laser was studied using graphene and MoS_2 SAs. The laser operated in the range of P_{abs} = 0.14...0.35 W because it was not very stable near the laser threshold and at higher absorbed pump powers due to the SA heating [39]. The emission of the PQS laser was linearly polarized, $\boldsymbol{E} \parallel N_m$.

The input-output dependences and typical laser emission spectra of the graphene and MoS_2 PQS Tm:KLuW WG lasers are shown in Fig. 6. In terms of average output power and slope efficiency, the 30% OC provided the best performance: The laser generated 24.9 mW at 1844.8 nm with η = 9.3% (for graphene SA) and 22.1 mW at a shorter wavelength of 1843.4 nm with slightly lower η of 8.5% (for MoS_2 SA). Considering the output power achieved in the CW mode at P_{abs} = 0.35 W, the Q-switching conversion efficiency η_{conv} was 16.6% and 14.7% for graphene and MoS_2 SAs, respectively. The reduction of η for the PQS WG laser as compared to the CW operation mode is due to the insertion loss of the SA (including the non-saturable losses for the graphene and MoS_2 films and Fresnel losses at the uncoated substrate). It is estimated as 11.9% and 10.7% for the graphene and MoS_2 SAs, respectively.

Regarding the laser emission spectra, see Fig. 6(b), higher output coupling corresponded to a slightly shorter emission wavelength in agreement with the quasi-three-level nature of the Tm^{3+} ion.

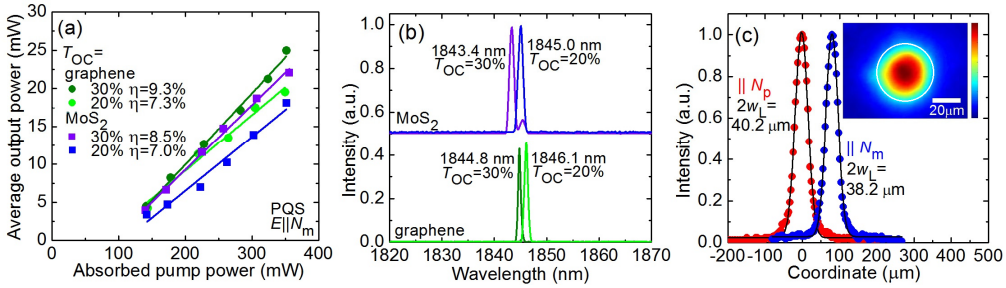

Fig. 6. Graphene and MoS_2 PQS Tm:KLuW channel WG lasers: (a) input-output dependences, η – slope efficiency, (b) typical laser emission spectra measured at maximum P_{abs}, (c) calibrated 1D intensity profiles of the laser mode at the output face of the WG along the N_m and N_p axes: *symbols* – experimental data, *curves* – Gaussian fits, *inset* – 2D mode profile, the *white circle* indicates the cladding (graphene SA, T_{OC} = 30%, P_{abs} = 0.35 W). The laser polarization is $\boldsymbol{E} \parallel N_m$.

The 1D intensity profiles of the laser mode along the horizontal ($\parallel N_m$-axis) and vertical ($\parallel N_p$-axis) directions are shown in Fig. 6(c). They are well fitted with a Gaussian distribution (quality of the fit R^2 >0.99) yielding the diameters of the laser mode $2w_L$ of 38.2 μm and 40.2 μm, respectively. Thus, the laser mode is well confined within the WG cladding indicated by a white circle at the inset of Fig. 6(c) showing a 2D mode profile. The M^2 (beam quality) parameter of the laser mode was determined by analysing its divergence as 1.20 ± 0.05 (for both horizontal and vertical directions).

According to the determined M^2 being close to unity and nearly-Gaussian 1D intensity profiles of the laser mode, Fig. 6(c), we conclude that the laser operated at the fundamental mode (LP_{01}). Within the step-index approximation, we calculated the normalized frequency $V = 2\pi a$N.A./λ_L = 2.4 ± 0.1 (N.A. = 0.035 is the numerical aperture of the WG, a = 20 μm is the WG core radius, λ_L is the laser wavelength). The cut-off V parameters for the $LP_{lm} = LP_{01}$ and LP_{11} (doubly degenerated) modes are 0 and 2.405, respectively. In our case, the generation of the LP_{11} modes is not observed probably to an additional effect of gain-guiding.

Optics EXPRESS

The pulse duration (determined as full width at half maximum, FWHM) $\Delta\tau$ and the pulse repetition frequency (PRF) were measured directly. The pulse energy, $E_{out} = P_{out}/PRF$, was calculated. In Fig. 7, we summarized the results regarding $\Delta\tau$, PRF and E_{out} for graphene and MoS_2 PQS Tm:KLuW WG lasers (for 30% OC).

The pulse characteristics were dependent on P_{abs}. This behaviour is typical for "fast" SAs contrary to the "slow" ones (e.g., Cr^{2+}:ZnS) and it is related to their dynamic bleaching [17]. "Fast" SAs such as graphene or MoS_2 are saturated by the laser intensity. With an increase of the pump power, the intracavity intensity on the SA ($I_{in} = X\cdot(2E_{out}/(\pi w_L^2\Delta\tau^*))$, where $X = (2 - T_{OC})/T_{OC}$ is the output-coupling factor and $\Delta\tau^* \approx 1.06\Delta\tau$ is the effective pulse duration assuming both Gaussian laser mode and temporal pulse profile) increases thus leading to larger modulation depth asymptotically approaching the α'_S value. This, in turn, will lead to an increase of the pulse energy and shortening of the pulse duration with the pump power. For $T_{OC} = 30\%$, the maximum intracavity laser intensity I_{in} on both SAs is ~0.19 MW/cm^2 being smaller than I_{sat}. Thus, the SA bleaching is indeed partial.

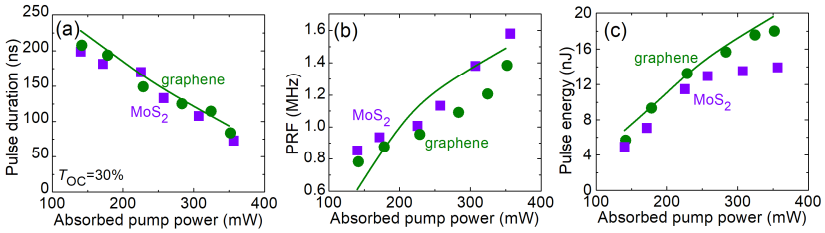

Fig. 7. Graphene and MoS_2 PQS Tm:KLuW channel WG laser: (a) pulse duration (FWHM), (b) pulse repetition frequency (PRF) and (c) pulse energy. *Symbols*: experimental data; *curves* – numerical calculation using the model from [17] for graphene-SA.

For $T_{OC} = 30\%$ and graphene SA, the pulse duration shortened from 208 to 88 ns, the PRF increased from 0.78 to 1.39 MHz and the pulse energy – from 5.7 to 18.0 nJ. The maximum peak power $P_{peak} = E_{out}/\Delta\tau$ thus reached 0.21 W. For the MoS_2-SA, $\Delta\tau$ shortened from 199 to 73 ns, the PRF increased from 0.85 to 1.58 MHz and E_{out} – from 4.9 to 14.0 nJ. The peak power was similar to that for the graphene-SA, P_{peak} = 0.19 W. A "saturation" of the dependence of the pulse energy on the pump power, Fig. 7(c), is an indication of the SA heating by the residual pump leading to a decreased α'_S.

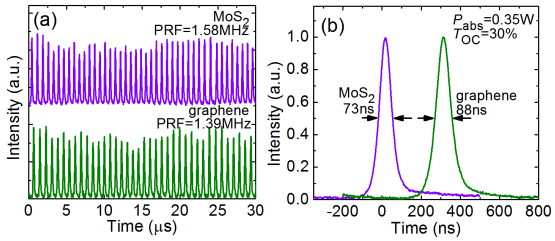

Fig. 8. Oscilloscope traces of (a) the typical pulse trains and (b) the shortest Q-switched pulses from the graphene and MoS_2 PQS Tm:KLuW channel WG lasers.

The pulse characteristics of the PQS WG laser were also calculated numerically using the model of a quasi-three-level laser medium and a "fast" SA described in [17,40]. The results for graphene-SA are shown in Fig. 7 as curves. The model reasonably describes the observed PQS behaviour. For the maximum P_{abs} = 0.35 W, it predicts the generation of 94 ns / 19.6 nJ pulses at a repetition rate of 1.49 MHz. The uncertainty in the calculated pulse characteristics is about 20%. The calculated results for the MoS_2-based SA were similar to those of graphene (within the indicated uncertainty) and thus they are not shown in Fig. 7.

Optics EXPRESS

The use of 20% OC resulted in a shorter pulse duration for both graphene- and MoS_2-SAs (due to the higher intracavity intensity on the SA I_{in} reaching ~0.27 MW/cm^2) albeit at lower pulse energy.

The oscilloscope traces of the shortest Q-switched pulses and the corresponding pulse trains from the graphene and MoS_2 PQS Tm:KLuW WG lasers are shown in Fig. 8. The Q-switching intensity instabilities were below 20% (measured over a time span of 1 ms) and they are attributed to the heating of the SA due to the non-absorbed pump radiation [39].

The output characteristics of the fs-DLW channel WG lasers PQS by graphene- and MoS_2-SAs are summarized in Table 3. The possibility to achieve shorter pulses with MoS_2 SA is explained by a larger fraction of the saturable loss to the small-signal absorption for this material (α'_S/α'_{SA} = 0.074) as compared to graphene (α'_S/α'_{SA} = 0.042) [19].

Table 3. Output Characteristics of the PQS Tm:KLuW Channel WG Lasers.

SA	T_{OC}, %	P_{out}, mW	η, %	η_{conv}, %	λ_L, nm	$\Delta\tau$, ns	PRF, MHz	E_{out}, nJ
graphene	20	19.5	7.3	18.1	1846.1	72	1.45	13.1
	30	24.9	9.3	16.6	1844.8	88	1.39	18.0
MoS_2	20	18.1	7.0	16.7	1845.0	66	1.51	12.0
	30	22.1	8.5	14.7	1843.4	73	1.58	14.0

4. Conclusion

Two-dimensional materials (graphene and few-layer MoS_2) are promising SAs for WG lasers emitting at ~2 μm. They enable the generation of sub-100 ns pulses with nJ-level energies at high repetition rates (MHz-range). A fs-DLW circular cladding channel WG laser based on monoclinic Tm:$KLu(WO_4)_2$ crystal is PQS by graphene and MoS_2 SAs. For graphene-SA, the best pulse characteristics are 88 ns / 18 nJ at a PRF of 1.39 MHz corresponding to an average output power of ~25 mW and a slope efficiency of ~9%. Using MoS_2 SAs, shorter pulses (down to 66 ns) are achieved.

The achieved results represent a significant improvement of the laser performance as compared to the previously reported Tm WG lasers PQS by 2D materials such as graphene or topological insulator [20–22] (cf. Table 1). In particular, we report on the highest output power and slope efficiency while maintaining sub-100 ns pulse duration.

Graphene and MoS_2 are interesting for PQS fs-DLW Tm surface waveguide lasers relying on evanescent field interaction [41]. In such a way, the limitation due to the heating of the SA by the residual pump will be diminished and the Q-switching conversion efficiency with respect to the CW regime will be enhanced. Pulsed operation with durations of few tens of ns is expected from such lasers. Such laser sources are potentially interesting for bio and environmental sensing applications.

Regarding the CW laser performance, we have achieved the highest output power for any fs-DLW Tm WG laser based on crystalline, ceramic or glassy material (cf. Table 2). Further power scaling was limited by the available pump power. Note that for most of the previously studied fs-DLW Tm WG lasers [34–38], Ti:Sapphire was used as a pump source. For further power scaling and for potential applications, it is desirable to fabricate WGs suitable for diode-pumping (e.g., by fiber-coupled AlGaAs laser diodes). In the case of high-power diodes with multimode fibers, a larger diameter of the WG cladding is necessary. According to the procedure described in Section 2.1, we have fabricated circular cladding WGs with a diameter of 100 μm. Such WGs are expected to provide spatially multimode laser output. Diodes with a single-mode fiber (whilst with a limited pump power) can be used for pumping the existing WGs. We plan to perform such studies in the future.

Funding

Ministerio de Economía y Competitividad (MAT2016-75716-C2-1-R (AEI/FEDER,UE), TEC 2014-55948-R, FIS2017-87970); Consejería de Educación, Junta de Castilla y León

Optics EXPRESS

(UIC016, SA046U16); Agència de Gestió d'Ajuts Universitaris i de Recerca (2017SGR755); Horizon 2020 Framework Programme (747055).

Acknowledgments

E. K. acknowledges financial support from the Generalitat de Catalunya under grants 2016FI_B00844, 2017FI_B100158 and and 2018FI_B200123. F. D. acknowledges additional support through the ICREA academia award 2010ICREA-02 for excellence in research. A. R. acknowledges funding from the European Union's Horizon 2020 research and innovation programme under the Marie Skłodowska-Curie Individual Fellowship Grant Agreement No. 747055. P. L. acknowledges financial support from the Government of the Russian Federation (Grant 074-U01) through ITMO Post-Doctoral Fellowship scheme.

References

1. K. Scholle, S. Lamrini, P. Koopmann, and P. Fuhrberg, "2 μm laser sources and their possible applications," in *Frontiers in Guided Wave Optics and Optoelectronics*, B. Pal, Ed. (Intech, 2010, pp. 471–500).
2. K. van Dalfsen, S. Aravazhi, C. Grivas, S. M. García-Blanco, and M. Pollnau, "Thulium channel waveguide laser with 1.6 W of output power and ~80% slope efficiency," Opt. Lett. **39**(15), 4380–4383 (2014).
3. W. Bolanos, F. Starecki, A. Benayad, G. Brasse, V. Ménard, J.-L. Doualan, A. Braud, R. Moncorgé, and P. Camy, "Tm:$LiYF_4$ planar waveguide laser at 1.9 μm," Opt. Lett. **37**(19), 4032–4034 (2012).
4. J. I. Mackenzie, S. C. Mitchell, R. J. Beach, H. E. Meissner, and D. P. Shepherd, "15 W diode-side-pumped Tm:YAG waveguide laser at 2 μm," Electron. Lett. **37**(14), 898–899 (2001).
5. D. P. Shepherd, D. J. B. Brinck, J. Wang, A. C. Tropper, D. C. Hanna, G. Kakarantzas, and P. D. Townsend, "1.9-μm operation of a Tm:lead germanate glass waveguide laser," Opt. Lett. **19**(13), 954–956 (1994).
6. N. Li, P. Purnawirman, Z. Su, E. Salih Magden, P. T. Callahan, K. Shtyrkova, M. Xin, A. Ruocco, C. Baiocco, E. P. Ippen, F. X. Kärtner, J. D. B. Bradley, D. Vermeulen, and M. R. Watts, "High-power thulium lasers on a silicon photonics platform," Opt. Lett. **42**(6), 1181–1184 (2017).
7. D. G. Lancaster, S. Gross, H. Ebendorff-Heidepriem, K. Kuan, T. M. Monro, M. Ams, A. Fuerbach, and M. J. Withford, "Fifty percent internal slope efficiency femtosecond direct-written Tm^{3+}:ZBLAN waveguide laser," Opt. Lett. **36**(9), 1587–1589 (2011).
8. M. Ams, G. D. Marshall, P. Dekker, J. A. Piper, and M. J. Withford, "Ultrafast laser written active devices," Laser Photonics Rev. **3**(6), 535–544 (2009).
9. F. Chen and J. R. Vázquez de Aldana, "Optical waveguides in crystalline dielectric materials produced by femtosecond-laser micromachining," Laser Photonics Rev. **8**(2), 251–275 (2014).
10. P. Loiko, J. M. Serres, X. Mateos, K. Yumashev, A. Yasukevich, V. Petrov, U. Griebner, M. Aguiló, and F. Díaz, "Subnanosecond Tm:KLuW microchip laser Q-switched by a Cr:ZnS saturable absorber," Opt. Lett. **40**(22), 5220–5223 (2015).
11. Q. Bao, H. Zhang, Y. Wang, Z. Ni, Y. Yan, Z. X. Shen, K. P. Loh, and D. Y. Tang, "Atomic-layer graphene as a saturable absorber for ultrafast pulsed lasers," Adv. Funct. Mater. **19**(19), 3077–3083 (2009).
12. W. B. Cho, J. H. Yim, S. Y. Choi, S. Lee, A. Schmidt, G. Steinmeyer, U. Griebner, V. Petrov, D.-I. Yeom, K. Kim, and F. Rotermund, "Boosting the nonlinear optical response of carbon nanotube saturable absorbers for broadband mode-locking of bulk lasers," Adv. Funct. Mater. **20**(12), 1937–1943 (2010).
13. S. Wang, H. Yu, H. Zhang, A. Wang, M. Zhao, Y. Chen, L. Mei, and J. Wang, "Broadband few-layer MoS_2 saturable absorbers," Adv. Mater. **26**(21), 3538–3544 (2014).
14. R. R. Nair, P. Blake, A. N. Grigorenko, K. S. Novoselov, T. J. Booth, T. Stauber, N. M. R. Peres, and A. K. Geim, "Fine structure constant defines visual transparency of graphene," Science **320**(5881), 1308 (2008).
15. G. Xing, H. Guo, X. Zhang, T. C. Sum, and C. H. A. Huan, "The Physics of ultrafast saturable absorption in graphene," Opt. Express **18**(5), 4564–4573 (2010).
16. F. Zhang, S. Han, Y. Liu, Z. Wang, and X. Xu, "Dependence of the saturable absorption of graphene upon excitation photon energy," Appl. Phys. Lett. **106**(9), 091102 (2015).
17. A. S. Yasukevich, P. Loiko, N. V. Gusakova, J. M. Serres, X. Mateos, K. V. Yumashev, N. V. Kuleshov, V. Petrov, U. Griebner, M. Aguiló, and F. Díaz, "Modelling of graphene Q-switched Tm lasers," Opt. Commun. **389**, 15–22 (2017).
18. H. Zhang, S. B. Lu, J. Zheng, J. Du, S. C. Wen, D. Y. Tang, and K. P. Loh, "Molybdenum disulfide (MoS_2) as a broadband saturable absorber for ultra-fast photonics," Opt. Express **22**(6), 7249–7260 (2014).
19. J. M. Serres, P. Loiko, X. Mateos, H. Yu, H. Zhang, Y. Chen, V. Petrov, U. Griebner, K. Yumashev, M. Aguiló, and F. Díaz, "MoS_2 saturable absorber for passive Q-switching of Yb and Tm microchip lasers," Opt. Mater. Express **6**(10), 3262–3273 (2016).
20. J. H. Lee, S. Gross, B. V. Cunning, C. L. Brown, D. Kielpinski, T. M. Monro, and D. G. Lancaster, "Graphene-based passive Q-switching of a Tm^{3+}:ZBLAN short-infrared waveguide laser," in *Conference on Lasers and Electro-Optics (CLEO)* (IEEE, 2014), paper P. JTu4A.128.

Optics EXPRESS

21. X. Jiang, S. Gross, H. Zhang, Z. Guo, M. J. Withford, and A. Fuerbach, "Bismuth telluride topological insulator nanosheet saturable absorbers for Q-switched mode-locked Tm:ZBLAN waveguide lasers," Ann. Phys. **528**(7–8), 543–550 (2016).
22. Y. Ren, G. Brown, R. Mary, G. Demetriou, D. Popa, F. Torrisi, A. C. Ferrari, F. Chen, and A. K. Kar, "7.8-GHz graphene-based 2-μm monolithic waveguide laser," IEEE J. Sel. Top. Quantum Electron. **21**(1), 395–400 (2015).
23. E. Kifle, X. Mateos, J. R. de Aldana, A. Ródenas, P. Loiko, S. Y. Choi, F. Rotermund, U. Griebner, V. Petrov, M. Aguiló, and F. Díaz, "Femtosecond-laser-written Tm:$KLu(WO_4)_2$ waveguide lasers," Opt. Lett. **42**(6), 1169–1172 (2017).
24. W. Bolaños, J. J. Carvajal, X. Mateos, E. Cantelar, G. Lifante, U. Griebner, V. Petrov, V. L. Panyutin, G. S. Murugan, J. S. Wilkinson, M. Aguiló, and F. Díaz, "Continuous-wave and Q-switched Tm-doped $KY(WO_4)_2$ planar waveguide laser at 1.84 μm," Opt. Express **19**(2), 1449–1454 (2011).
25. E. Kifle, X. Mateos, P. Loiko, S. Y. Choi, J. E. Bae, F. Rotermund, M. Aguiló, F. Díaz, U. Griebner, and V. Petrov, "Tm:KY_1-x-yGdxLuy$(WO_4)_2$ planar waveguide laser passively Q-switched by single-walled carbon nanotubes," Opt. Express **26**(4), 4961–4966 (2018).
26. V. Petrov, M. C. Pujol, X. Mateos, Ò. Silvestre, S. Rivier, M. Aguiló, R. M. Solé, J. H. Liu, U. Griebner, and F. Díaz, "Growth and properties of $KLu(WO_4)_2$, and novel ytterbium and thulium lasers based on this monoclinic crystalline host," Laser Photonics Rev. **1**(2), 179–212 (2007).
27. E. Kifle, P. Loiko, X. Mateos, J. R. Vázquez de Aldana, A. Ródenas, U. Griebner, V. Petrov, M. Aguiló, and F. Díaz, "Femtosecond-laser-written hexagonal cladding waveguide in Tm:$KLu(WO_4)_2$: μ-Raman study and laser operation," Opt. Mater. Express **7**(12), 4258–4268 (2017).
28. H.-D. Nguyen, A. Ródenas, J. R. Vázquez de Aldana, J. Martínez, F. Chen, M. Aguiló, M. C. Pujol, and F. Díaz, "Heuristic modelling of laser written mid-infrared $LiNbO_3$ stressed-cladding waveguides," Opt. Express **24**(7), 7777–7791 (2016).
29. R. Lan, P. Loiko, X. Mateos, Y. Wang, J. Li, Y. Pan, S. Y. Choi, M. H. Kim, F. Rotermund, A. Yasukevich, K. Yumashev, U. Griebner, and V. Petrov, "Passive Q-switching of microchip lasers based on Ho:YAG ceramics," Appl. Opt. **55**(18), 4877–4887 (2016).
30. A. C. Ferrari, J. C. Meyer, V. Scardaci, C. Casiraghi, M. Lazzeri, F. Mauri, S. Piscanec, D. Jiang, K. S. Novoselov, S. Roth, and A. K. Geim, "Raman spectrum of graphene and graphene layers," Phys. Rev. Lett. **97**(18), 187401 (2006).
31. L. M. Malard, M. A. A. Pimenta, G. Dresselhaus, and M. S. Dresselhaus, "Raman spectroscopy in graphene," Phys. Rep. **473**(56), 51–87 (2009).
32. N. T. McDevitt, J. S. Zabinski, M. S. Donley, and J. E. Bultman, "Disorder-induced low-frequency Raman band observed in deposited MoS_2 films," Appl. Spectrosc. **48**(6), 733–736 (1994).
33. J. A. Caird, S. A. Payne, P. R. Staber, A. J. Ramponi, L. L. Chase, and W. F. Krupke, "Quantum electronic properties of the $Na_3Ga_2Li_3F_{12}:Cr^{3+}$ laser," IEEE J. Quantum Electron. **24**(6), 1077–1099 (1988).
34. D. G. Lancaster, S. Gross, A. Fuerbach, H. E. Heidepriem, T. M. Monro, and M. J. Withford, "Versatile large-mode-area femtosecond laser-written Tm:ZBLAN glass chip lasers," Opt. Express **20**(25), 27503–27509 (2012).
35. F. Fusari, R. R. Thomson, G. Jose, F. M. Bain, A. A. Lagatsky, N. D. Psaila, A. K. Kar, A. Jha, W. Sibbett, and C. T. A. Brown, "Lasing action at around 1.9 μm from an ultrafast laser inscribed Tm-doped glass waveguide," Opt. Lett. **36**(9), 1566–1568 (2011).
36. Y. Ren, G. Brown, A. Ródenas, S. Beecher, F. Chen, and A. K. Kar, "Mid-infrared waveguide lasers in rare-earth-doped YAG," Opt. Lett. **37**(16), 3339–3341 (2012).
37. J. Morris, N. K. Stevenson, H. T. Bookey, A. K. Kar, C. T. A. Brown, J.-M. Hopkins, M. D. Dawson, and A. A. Lagatsky, "1.9 μm waveguide laser fabricated by ultrafast laser inscription in Tm:Lu_2O_3 ceramic," Opt. Express **25**(13), 14910–14917 (2017).
38. Y. Y. Ren, S. J. Beecher, G. Brown, A. Ródenas, A. Lancaster, F. Chen, and A. K. Kar, "Q-switched mode-locking of a mid-infrared Tm:YAG waveguide laser with graphene film," *in Conference on Lasers and Electro-Optics Pacific Rim* (IEEE, 2013), paper 1–3.
39. J. M. Serres, P. Loiko, X. Mateos, K. Yumashev, U. Griebner, V. Petrov, M. Aguiló, and F. Díaz, "Tm:$KLu(WO_{(4)})_{(2)}$ microchip laser Q-switched by a graphene-based saturable absorber," Opt. Express **23**(11), 14108–14113 (2015).
40. E. Kifle, X. Mateos, P. Loiko, V. Petrov, U. Griebner, M. Aguiló, and F. Díaz, "Graphene Q-switched Tm:$KY(WO_4)_2$ waveguide laser," Laser Phys. **27**(4), 045801 (2017).
41. E. Kifle, P. Loiko, J. R. V. de Aldana, C. Romero, A. Ródenas, S. Y. Choi, J. E. Bae, F. Rotermund, V. Zakharov, A. Veniaminov, M. Aguiló, F. Díaz, U. Griebner, V. Petrov, and X. Mateos, "Passively Q-switched fs-laser-written thulium waveguide laser based on evanescent field interaction with carbon nanotubes," Photon. Res. **6**(10), 971–980 (2018).